



Diagnostics of fast formation of distributed plasma discharges using X-band microwaves

X. Xiang, B. Kupczyk, J. Booske, and J. Scharer

Citation: [Journal of Applied Physics](#) **115**, 063301 (2014); doi: 10.1063/1.4865275

View online: <http://dx.doi.org/10.1063/1.4865275>

View Table of Contents: <http://scitation.aip.org/content/aip/journal/jap/115/6?ver=pdfcov>

Published by the [AIP Publishing](#)



Re-register for Table of Content Alerts

Create a profile.



Sign up today!



Diagnostics of fast formation of distributed plasma discharges using X-band microwaves

X. Xiang,^{a)} B. Kupczyk, J. Booske, and J. Scharer
*Department of Electrical and Computer Engineering, University of Wisconsin, Madison,
 Wisconsin 53705, USA*

(Received 7 December 2013; accepted 29 January 2014; published online 12 February 2014)

We present measurements of high power (25.7 kW), pulsed (800 ns), X-band (9.382 GHz) microwave breakdown plasmas, including reflected power measurements, mixer reflected amplitude and phase measurements, optical emission spectroscopy (OES) measurements, and an analysis that estimates the average electron density and electron temperature. In addition, a six-region, 1-D model was used to determine plasma parameters and compare with the experimental results. The experimental results show that using a 43 Hz repetition rate with an 800 ns pulse, fast (<300 ns) breakdown occurs in neon measured between 50 Torr and 250 Torr, producing plasma that lasts for over 7 μ s. It also leads to large microwave reflections (70%) and an on-axis transmission attenuation of -15 dB. Moreover, a comparison between a 1-D model and mixer measurements shows that at 100 Torr, the neon plasma electron density peaked at $2 \times 10^{12} \text{ cm}^{-3}$, and the electron temperature peaked at 2.5 eV assuming a Maxwellian distribution. The addition of 2% Ar in Ne reduced the breakdown time and allowed OES measurements to determine the effective electron temperature. OES measurements of mixed (Ne/Ar: 98/2) argon line ratios (420.1 nm/419.8 nm) were used to determine the average effective electron temperature $T_{e(\text{eff})} = 1.2 \text{ eV}$, averaged over the entire 7 μ s plasma lifetime. They indicate that the electron energy distribution was not Maxwellian but, instead, tended towards a Druyvesteyn character. © 2014 AIP Publishing LLC.
[\[http://dx.doi.org/10.1063/1.4865275\]](http://dx.doi.org/10.1063/1.4865275)

I. INTRODUCTION

Research on continuous wave (CW) and pulsed microwave breakdown in air and noble gases has been conducted for some time since the pioneering work of MacDonald¹ in microwave cavities. Given the technical advances including optical emission spectroscopy (OES) and fast ICCD (Intensified Charge Coupled Device) imaging that can be used to examine pulsed breakdown, we have further examined the conditions and plasma characteristics that enable rapid (<300 ns) breakdown in noble gas plasmas. This was carried out as a basic study of distributed plasma breakdown and plasma evolution in a large cylindrical vacuum chamber (having a diameter of 14.6 cm and a length of 15.2 cm). To achieve this goal and better understand the plasma formation and decay under different conditions including different gas compositions, pressure, pulse length, and repetition rate, non-invasive diagnostic measurements and modeling of the plasma density, temperature, and transient spatial evolution were carried out.

To examine the plasma breakdown, we used pulsed (800 ns), high power (25.7 kW) X-band (9.382 GHz) microwaves in a noble gas (neon) and Ne/Ar mixes that enhanced the plasma breakdown and discharge. We also carried out experiments and 1-D modeling of the plasma to investigate its parameters, including the effective plasma density, electron temperature, and spatial extent. We examined an incident single pulse of microwave power at 25.7 kW in our X-band waveguide propagating through 0.953 cm thick,

14.6 cm diameter polycarbonate windows spaced 15.2 cm apart that was evacuated to 10^{-3} Torr and filled with neon gas to 100 Torr. We found that single shot breakdown did not occur near the first window where the electric field strengths were highest. However, when repetitive pulses were sent with a 43 Hz repetition rate, breakdown in neon and Ne/Ar gas mixes did occur. For this study, a working definition of breakdown was used. Specifically, breakdown referred to the occurrence of a plasma discharge with sufficient density and size to emit a detectable intensity of visible light emission and to reflect a significant fraction of the incident microwave power.

The purpose of our study was to examine characteristics of rapid plasma breakdown in distributed, laterally unbounded volumes by high power microwave pulses.² There are several features of this study that differed from previous investigations. Our experiments used short pulses, which generally require higher field strengths for breakdown than experiments using a CW microwave source,¹ where the peak fields occurred in space between microwave cavity walls. As a result of the pulsed power condition, the plasma in our studies rapidly changed as it grew during the pulse and decayed after the short microwave pulse was turned off. Thus, the plasma size, density, temperature, and luminosity all varied rapidly in time. Unlike some previous microwave plasma studies^{3,4} conducted in waveguides, we used the previously described comparatively large cylindrical chamber to examine the plasma evolution without the influence of metallic conducting waveguide boundaries. As a result, the diffuse nature of the plasma in the transition between the X-band waveguide to the cylindrical, over-moded chamber

^{a)}Electronic mail: xxiang3@wisc.edu

introduced additional factors to consider. For example, the use of a polycarbonate window between the X-band waveguide and the plasma chamber as well as the abrupt change in lateral dimensions between the waveguide and the window-and-chamber caused wave impedance mismatches, which resulted in a $\sim 5\%$ power reflection that needed to be considered in determining the reflected power arising from plasma creation. Furthermore, the abrupt change from a fundamental mode waveguide to the window-and-chamber modified the transverse electric field pattern from the incident, simplified TE_{10} mode distribution.

In this paper, we describe and discuss plasma reflection and absorption power measurements and plasma parameter diagnostic results using an 800 ns pulse with a 43 Hz repetition rate at 100 Torr. A six-region, 1-D model was developed to estimate the plasma temperature and density, in addition to five diagnostics of the plasma. Section I discusses the plasma reflected power measurements. Section II discusses determination of the gas temperature of the microwave plasma using an OES method. Section III shows fast-gated (50 ns) ICCD images and analyses to characterize the plasma's spatial evolution. Section IV compares the microwave reflection mixer experimental results and 1-D model to determine spatially averaged peak plasma parameters. Section V discusses OES line ratio studies to determine the plasma effective temperature and nature of the electron energy distribution. Finally, summaries and comparisons of the diagnostic results are discussed.

II. EXPERIMENTAL CONFIGURATION

The X-band magnetron source launched 25.7 kW microwave pulses at 9.382 GHz using the experimental system shown in Fig. 1. The pulse width was 800 ns, and could be repeatedly pulsed at different rates. In this paper, all the experiments reported used a 43 Hz repetition rate. Two X-band directional couplers were used to detect the amplitude and phase of the incident and reflected signals by mixing with a sample of the incident signal through microwave diodes and mixers. Isolation of the reflected signal from the incident pulse was accomplished by a three-port circulator.

A cylindrical stainless steel chamber with two side ports was used as the discharge chamber, which was enclosed with 0.953 cm thick polycarbonate windows on both ends that could be pumped down to a base pressure of 10^{-3} Torr with a turbo pump and a scroll pump before filling with neon to the 10 to 300 Torr range. The discharge chamber was followed by an absorbing or matched load end wall chamber that had the same size as the discharge chamber, filled with a microwave absorber with <20 dB reflection, assuring that the transmitted power was absorbed via the matched load section. The mass flow controller adjusted the gas flow rate. There was a coaxial probe that could be moved in the vertical direction in the cylindrical chamber centrally located at $z = 31.1$ cm from the first polycarbonate window ($z = 0$) to monitor the on-axis transmitted wave amplitude and phase via a microwave mixer that used a sample of the incident signal as a reference.

In addition, an Andor iStar 734 ICCD detector capable of a 2 ns gated time window was used to take temporal plasma images from a side port angled at 62° from the axis or end on with a 32 dB transmission screen located at $z = 35.6$ cm, which provided images of the rapid time evolution of the plasma formation and decay. An Acton SpectraPro 500i spectrometer was used with the ICCD to measure the plasma's emission spectrum to determine the gas temperature and the effective electron temperature.

III. WAVE-PLASMA-DIELECTRIC MODEL

In order to model the experimental configuration, a simplified six-region, 1-D model was developed. This was done in order to obtain approximate values for the plasma density and effective electron temperature and minimize 2- and 3-D effects of the plasma evolution and wave mode character that would require much more extensive computational modeling and measurements. As shown in Fig. 2, each region was labeled with the thickness that was measured in the experimental setup. According to our ICCD plasma images and microwave reflected power measurements, once the plasma was formed, it extended well beyond the incident X-band waveguide port and resulted in very large reflections,

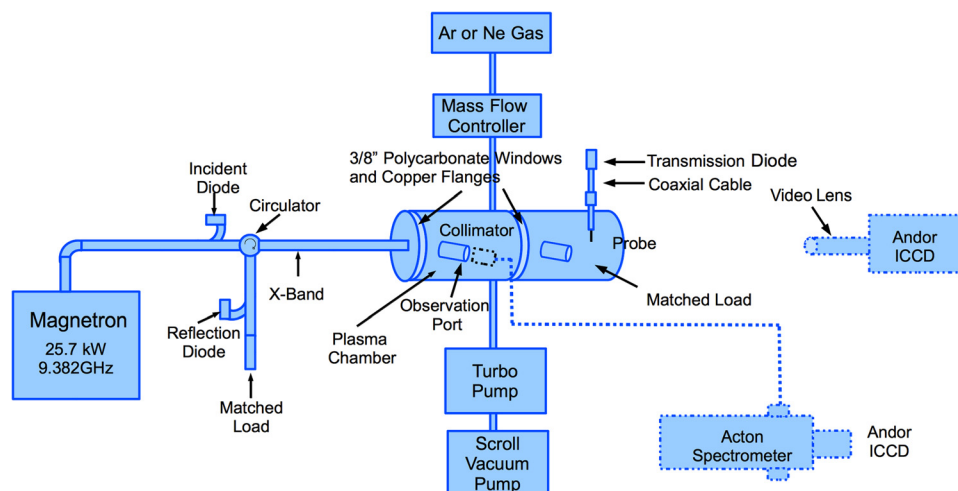


FIG. 1. Experimental configuration.

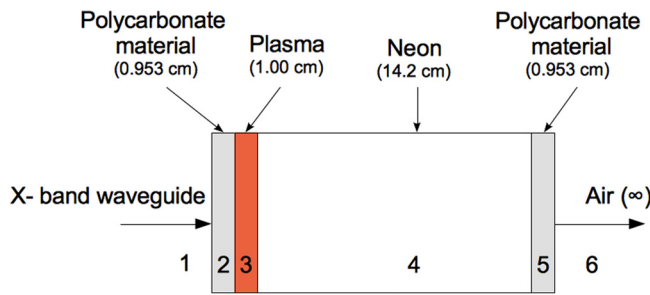


FIG. 2. Six-region, 1-D model.

which were over 70% of the total reflection. For comparison, we determined a reference condition corresponding to 100% reflection of all microwave power transmitted through the polycarbonate window by placing a copper disk against the downstream side of the first polycarbonate window. The voltage recorded on the reflected power diode detector when the copper disk was inserted, therefore, provided a 100% reflecting reference signal. The peak diode detector voltage observed with the plasma corresponded to 70% of this 100%-reflection reference condition. We interpreted this large reflection and the fact that the lateral size of the discharge exceeded the incident x-band waveguide dimensions as evidence supporting the reasonableness of characterizing the plasma with an effective 1-D slab model for the purpose of estimating the plasma density and electron temperature.

At higher and atmospheric pressures between 10 and 760 Torr, the plasma will be highly collisional. Thus, it can be modeled as a collisional dielectric medium and the dielectric constant can be expressed as⁵

$$\epsilon_p = \epsilon_0 \left[1 - \frac{\omega_p^2}{\omega(\omega - i\nu_{en})} \right], \quad (1)$$

where ϵ_p is the plasma dielectric constant, ω_p is the plasma frequency, and ν_{en} is the electron-neutral collision frequency in this 1-D model. Using these assumptions, one can apply electromagnetic wave equations and boundary conditions (see Appendix) together with the dielectric function for a highly collisional plasma to predict the microwave reflection coefficient as a function of gas pressure and assumed values for the plasma density, thickness, and Maxwellian electron temperature. Comparison with the experimentally measured reflection coefficient enabled us to infer values for the effective plasma frequency and electron temperature in the experiment. Figure 3 is an example of the power reflection coefficient, $|\Gamma|^2$, from the polycarbonate material into the X-band waveguide predicted by assuming a uniform plasma thickness of 1 cm at 100 Torr. The maximum value for the plasma thickness was estimated by observing optical light images that used the ICCD mounted on one of the side ports. Note that the model predicts a substantial power reflection coefficient, $|\Gamma|^2 (>70\%)$, similar to what was observed in the experiments, for values of $\omega_p/\omega > 1.5$ and $T_e < 3$ eV. In the no-plasma case, this simplified six-region 1-D wave model predicts a wave field magnitude reflection coefficient of $|\Gamma|=0.15$, which is comparable to the measured value of $|\Gamma|=0.17$ when plasma was not formed. The detailed

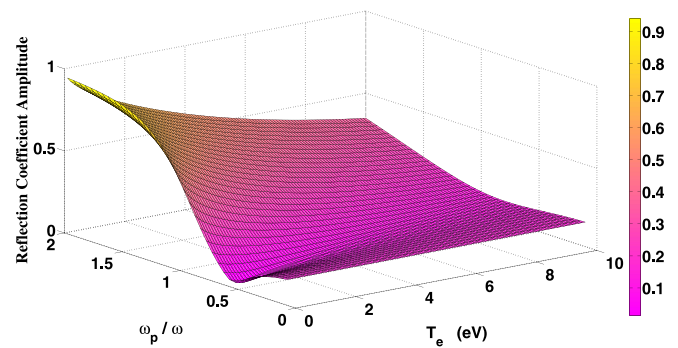


FIG. 3. Reflection coefficient (from first polycarbonate window to X-band waveguide) amplitude simulation for neon plasma at 100 Torr assuming the plasma is uniform and the plasma thickness is 1 cm.

electromagnetic equations and boundary conditions can be found in the Appendix.

IV. EXPERIMENTAL RESULTS

A. Reflected power measurements

The transmission dipole probe (see Fig. 1) was located in the transverse and vertical center of the cylindrical chamber at $z = 31.1$ cm from the first polycarbonate window located at $z = 0$ and could be adjusted vertically. As a localized sensor, it did not measure the total transmitted power. However, three-dimensional electromagnetic simulations suggested that it was useful as an indication of transmitted power since even though the chamber is over-moded, the excitation conditions resulted in a significant fraction of the wave energy peaking near the axis. In contrast, the total reflected power was measured with a directional coupler coupled to the incident X-band waveguide and was a more accurate measurement for comparison with our 1-D model's predictions. This premise is supported by observing that the plasma discharge light emission images after breakdown extend well beyond the incident X-band aperture. Measuring the reflected power under different gas mix and pressure conditions provided information regarding the breakdown time and the amplitude of plasma reflection coefficient. As previously described, we determined the total reflected power reference by covering the entire downstream surface of the first polycarbonate window with a copper disk. This method intrinsically accounted for the small skin effect absorption losses from the conductors and the dielectric losses from the polycarbonate. We then measured the reflected power for a neon plasma and for a mixed Ne/Ar (98/2) plasma case. Figure 4 compares the reflected power for different plasma cases with the total reflected power obtained with the copper disk.

As shown in Fig. 4, the calibrated total reflected power with the copper disk is 73.5 dBm, slightly less (-0.6 dB = 4%) than the incident power (74.1 dBm). When plasma was formed, the reflected power increased substantially compared to the case where only the polycarbonate windows and chamber were present without plasma formation. For both Ne and a Ne/Ar (98/2) mix (determined by our calibrated mass flow controllers) plasmas, the reflected power was 70% of the total reflected power reference condition. In addition, for pure neon,

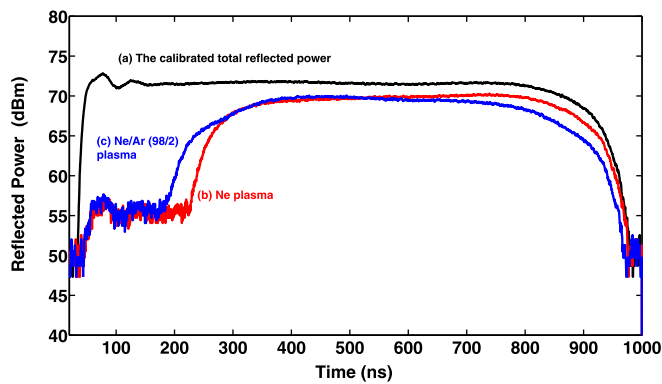


FIG. 4. Time resolved reflected power study for different plasmas and copper disk cases. (a) Black represents the calibrated total reflected power measured with a copper disk after the incident X-band waveguide and the first polycarbonate window. (b) Red represents reflected power in pure neon. (c) Blue represents reflected power in mixed neon and argon gas (Neon/Argon = 98:2). Both plasmas are formed at 100 Torr with a 43 Hz repetition rate.

the gas breakdown occurred at 250 ns into the pulse and for the Ne/Ar (98/2) case that allows Penning ionization processes,^{1,6} the breakdown time is reduced to 200 ns. Thus, we observed that Ne/Ar Penning gas mixes resulted in a more rapid plasma breakdown time than for neon alone.

B. Gas temperature measurements

One of the important plasma temperatures to characterize for the microwave plasma is the translational temperature T_{trans} , which describes the translational velocity distributions of the N_2 molecules and N^{2+} ions in the plasma. T_{trans} is often simply referred to as the gas temperature. Optical emission spectra have been widely used to obtain the gas temperature.^{7,8} In particular, by fitting the measured nitrogen lines with the SPECAIR^{9–11} model, the rotational temperature can be obtained. For our high pressure plasmas, since the collision rates between species are high, the translational temperatures of neutrals and ions are about equal, and $T_{\text{trans}} \approx T_{\text{rot}}$ can be assumed because the rotational relaxation time is quite fast.¹² Therefore, the gas temperature was assumed equal to the rotational temperature.

To obtain the gas temperature of the neon microwave plasma, we added 4.8% nitrogen into the system and then measured the 336 nm, 357 nm, and 375 nm neutral spectral lines. Because of our high operating pressure at 100 Torr, collisional equilibrium was assumed between nitrogen and neon so that the nitrogen gas temperature was equal to the neon gas temperature. At 100 Torr, each of the three nitrogen lines yielded a rotational temperature of 350 ± 50 K obtained by fitting with the SPECAIR model. Figure 5 is an example illustrating how well the 350 ± 50 K SPECAIR model fitted the measured 357 nm $\text{N}_2^{(2+)}$ nitrogen line. Further studies obtained by varying the pressure from 10 Torr to 180 Torr showed that the gas temperature varied only slightly (50 K) in this pressure range.

C. Plasma images

An Andor iStar 734 ICCD camera was used to take plasma images through the angled (62 degrees) side port of

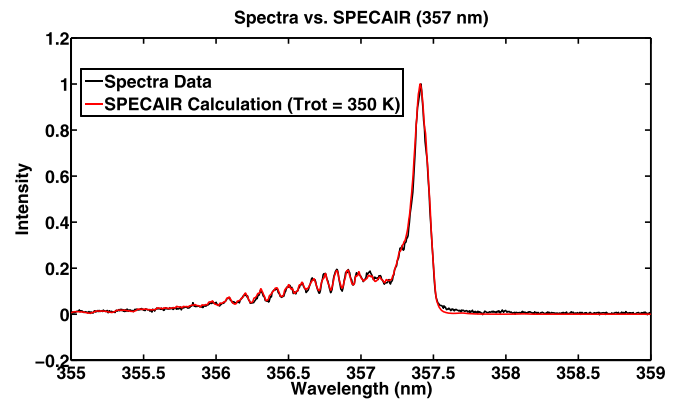


FIG. 5. The fitting of $\text{N}_2^{(2+)}$ 357 nm line to determine T_{gas} . Black represents spectra data by adding small amount of nitrogen into neon, and red represents the SPECAIR simulation when $T_{\text{rot}} = 350$ K.

the discharge chamber. As shown in Fig. 6, the discharge images start as a small ball at around 300 ns, and then grow larger while developing smaller finger-type structures at the upper and lower edges. After 900 ns, the plasma light

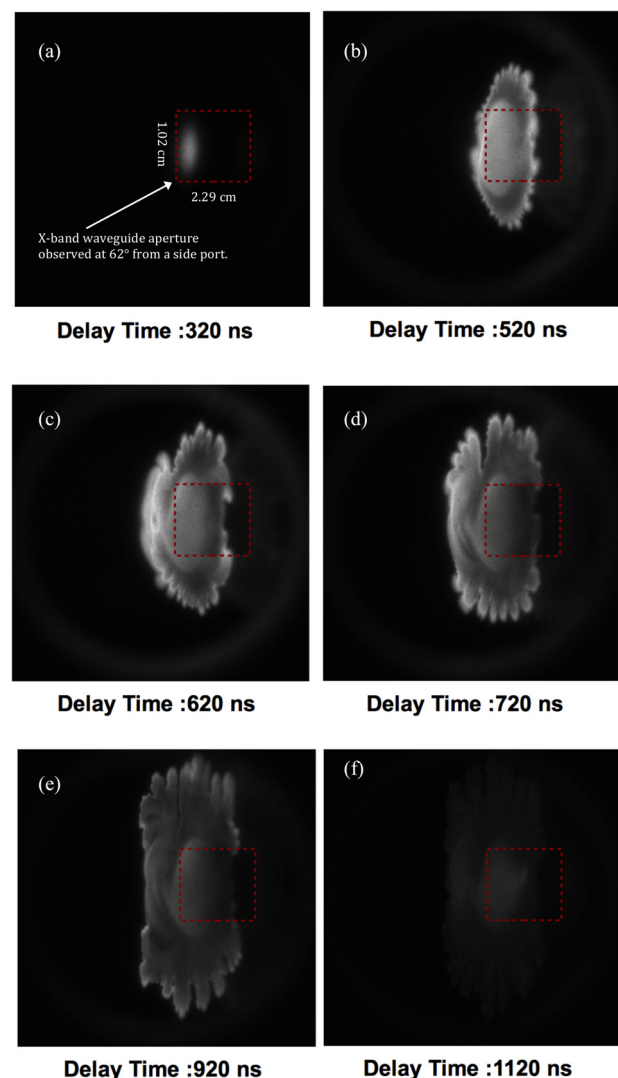


FIG. 6. ICCD images showing time-resolved neon plasma formation and decay process at 100 Torr. The exposure time for each picture is 50 ns, and the gain is 200. These pictures are taken from the side port (62°). The red dashed box is the X-band waveguide port.

emission images get dimmer and are extinguished at $7 \mu\text{s}$. All pictures in Fig. 6 were taken with an exposure time of 50 ns and a gain of 200. The plasmas for these images were obtained with pure neon at 100 Torr with a 43 Hz pulse repetition frequency. The substantial microwave reflections from the plasma that were observed to extend well beyond the X-band waveguide perimeter support the use of a 1-D model to obtain estimates for the effective plasma density and electron temperature caused by microwave breakdown.

D. Mixer experiment

By comparing the amplitude and phase of the measured wave reflection coefficient to the predictions of the six-region, 1-D model, effective plasma parameters such as density, temperature, and collision frequency could be estimated. To determine the phase of the reflection coefficient, we carried out a mixer quadrature experiment, which involved two steps. The first step was to use the incident signal as the reference and then mix the reflected signal with it using a microwave mixer, to obtain the mixed signal τ_1 . Then, we introduced a 90° phase shift in the incident signal to obtain the mixed signal τ_2 as follows:

$$\tau_1 = \text{Re}[A_i A_r e^{j(\phi_r - \phi_i)}], \quad (2a)$$

$$\tau_2 = \text{Re}[A_i A_r e^{j(\phi_r - \phi_i - \frac{\pi}{2})}]. \quad (2b)$$

The phase of the reflection coefficient was then obtained as

$$\phi_r - \phi_i = \arctan\left(\frac{\tau_2}{\tau_1}\right). \quad (3)$$

Since the measured mixed reflection signals were not at the same waveguide-to-polycarbonate terminal plane as where the six-region 1-D model was evaluated, a phase correction between the mixer location (on a reflected port, see Fig. 1) and the polycarbonate plane was made. We used a network analyzer to measure the phase difference between the mixer port and the waveguide-polycarbonate interface. Since all the components, including the X-band waveguides and microwave circulator were linear, the phase differences measured via the network analyzer were the same when plasma was formed. The phase difference correction was subtracted from the measured values at the diode to extract a phase shift that was referred to the phase at the X-band waveguide-to-polycarbonate plane that was compared with the amplitude and phase of the six-region, 1-D model. The amplitude of the reflection coefficient was obtained from the power measurement by the calibrated diodes as

$$|\Gamma_R| = \left| \sqrt{\frac{P_R}{P_I}} \right|. \quad (4)$$

By comparing the measured amplitude and phase of the reflection coefficient with the prediction of the model (Eqs. (A1)–(A20) in Appendix), the average plasma density and electron temperature were estimated. Figure 7 shows the plasma parameters for neon plasma at 100 Torr by assuming the maximum plasma thickness was 1 cm and using the neon

collisional cross section¹³ as a linear function of electron temperature between 1 and 5 eV.

Using the results from the mixer experiment, we estimated that the maximum effective plasma density was $2 \times 10^{12} \text{ cm}^{-3}$, and the maximum effective Maxwellian electron temperature was 2.5 eV, as shown in Fig. 7 at 380 ns. Correspondingly, the maximum $\omega_p/\omega = 1.4$ and maximum $\nu_{en}/\omega = 1.1$. These peak values are comparable with highly collisional model microwave plasma properties.^{14,15} It is noted that the results shown in Fig. 7 were obtained by fixing the plasma thickness as 1 cm at all times in the model. But, in reality, the plasma thickness changed with time. Similarly, the model presented in this section assumed a Maxwellian distribution, but the electron energy distribution might lie between Maxwellian and Druyvesteyn distribution in this highly collisional and unconfined plasma. Therefore, as stated previously, the parameter values are all effective values, associated with this and other simplifications assumed in the 1-D model. Nevertheless, they provide a useful estimate of the plasma density and electron temperature associated with the breakdown discharges observed in our experiments.

E. OES line ratio study

OES has been widely used for noninvasive plasma diagnostics. Line ratio methods are used to obtain plasma parameters such as electron temperature and plasma density. Boffard

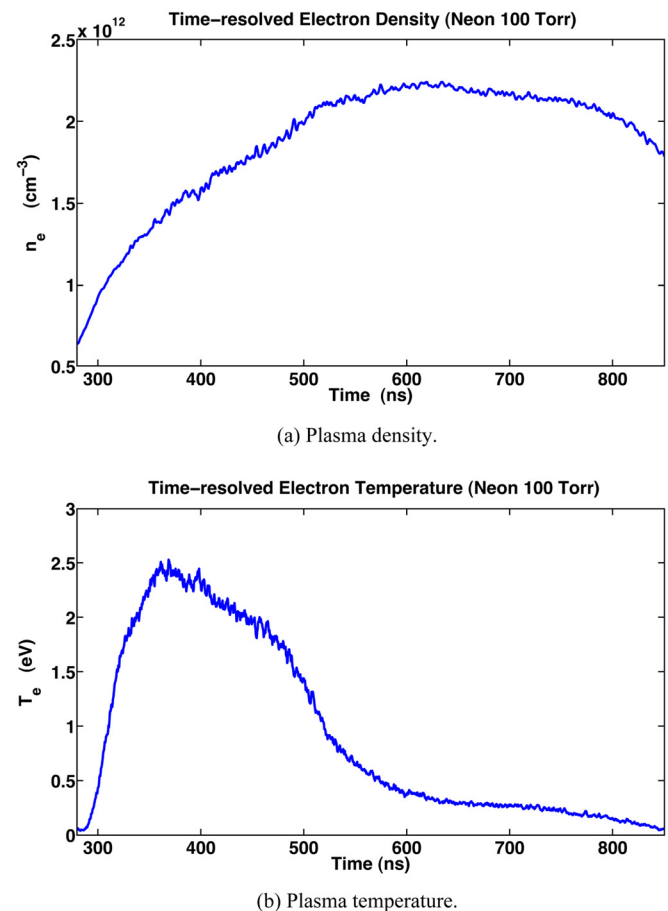


FIG. 7. Neon plasma parameters at 100 Torr estimated from mixer measurements with an assumed 1 cm thickness.

and Wendt¹⁶ have introduced an argon line pair ratio 420.1 nm/419.8 nm to estimate the effective electron temperature in an argon plasma. In Ref. 16, the results obtained from the line ratio method match very well with the results measured by a Langmuir probe in an inductively coupled RF plasma. To

apply this method in our system, we extended their corona emission model by including excitations from the resonance levels ($1s_2$ and $1s_4$), which are ignored in lower pressure plasmas due to the very short resonance state lifetimes. Thus, the extended corona emission photon flux model can be written as

$$\frac{\Phi_{420.1 \text{ nm}}}{\Phi_{419.8 \text{ nm}}} = \frac{k_{420.1 \text{ nm}}^g(T_{e(\text{eff})}) + \left(\frac{n_m}{n_o}\right)k_{420.1 \text{ nm}}^m(T_{e(\text{eff})}) + \left(\frac{n_r}{n_o}\right)k_{420.1 \text{ nm}}^r(T_{e(\text{eff})})}{k_{419.8 \text{ nm}}^g(T_{e(\text{eff})}) + \left(\frac{n_m}{n_o}\right)k_{419.8 \text{ nm}}^m(T_{e(\text{eff})}) + \left(\frac{n_r}{n_o}\right)k_{419.8 \text{ nm}}^r(T_{e(\text{eff})})}, \quad (5)$$

where Φ is the photon emission rate (photons/s); n_o , n_m , and n_r are the number density in ground state, metastable ($1s_3$ and $1s_5$), and resonance levels; k_{ij}^l represents the emission rate for a particular $i \rightarrow j$ transition due to electron-impact excitation of atoms initially in the lower level l (l can be ground state, metastable level and resonance level) and

$$k_{ij}^l(T_{e(\text{eff})}) = \sqrt{\frac{2}{m_e}} \int_0^\infty Q_{ij}^l(E) f_e(E; T_{e(\text{eff})}) \sqrt{E} dE, \quad (6)$$

where m_e is the electron mass, Q_{ij}^l is the $i \rightarrow j$ optical emission cross section for excitation from level l , and f_e is the electron energy distribution function (EEDF).

Note that the extended corona model requires knowledge of the number density in ground, metastable, and resonance levels. The number density in the ground state level is straightforwardly obtained from the gas temperature measurements and $n_o = 2.76 \times 10^{18} \text{ cm}^{-3}$ for a 100 Torr plasma with $T_{\text{gas}} = 350 \text{ K}$. As for the metastable density values, Donnelly¹⁷ developed a model to estimate them. By equating the production and loss rates, and ignoring the diffusion loss, the metastable-to-neutral-number-density-ratio n_m/n_o can be expressed as a function of the effective electron temperature $T_{e(\text{eff})} = \frac{2}{3} \langle E_e \rangle$

$$\frac{n_m}{n_o} = \frac{1.2T_{e(\text{eff})}^{-0.62} \exp\left(-\frac{20.11}{T_{e(\text{eff})}}\right)}{1.16 + 0.59T_{e(\text{eff})} - 0.03T_{e(\text{eff})}^2}. \quad (7)$$

For the resonance number density n_r , we assumed that $n_r = 0.6 n_m$, based on the angular momentum relationship between the two levels.¹⁶

Thus, by combining the corona and metastable number density models, given the 420.1 nm/419.8 nm line ratio, we estimated the effective electron temperature by iteration using Eqs. (5) and (7). We chose to start with an initial estimate for n_m/n_o in Eq. (5) to obtain $T_{e(\text{eff})}$, then used this $T_{e(\text{eff})}$ to determine a new n_m/n_o value from Eq. (7). We used this procedure because Eq. (5) is more tolerant of errors in n_m/n_o than Eq. (7) is in estimating $T_{e(\text{eff})}$. This is because Eq. (5) is a linear function of n_m/n_o , while Eq. (7) is an exponential function of $T_{e(\text{eff})}$.

Figure 8 shows the 420.1 nm and 419.8 nm line spectra with a 200 ICCD gain and a 10 μs exposure time, which

covered the whole 7 μs lifetime of the plasma, accumulated 800 times. To determine the line ratio, we applied a Gaussian fit to obtain the peak area (the area enclosed between the peak and the peak base). For a discharge in a gas mixture of Ne/Ar at a ratio of 98:2 and pressure of 100 Torr with a 10 μs observation gate, the line ratio was 2.0.

However, the iteration procedure did not converge under the assumption of a Maxwellian electron energy distribution. Thus, a more general form to represent the EEDF¹⁸ was used

$$f(E; T_{e(\text{eff})}) = c_1 T_{e(\text{eff})}^{-3/2} \sqrt{E} e^{-c_2 \left(\frac{E}{T_{e(\text{eff})}}\right)^x}, \quad (8)$$

where $x=1$ corresponds to a Maxwellian EEDF and $x=2$ corresponds to a Druyvesteyn EEDF.

By choosing $x=1.3$, the iteration converged and resulted in $T_{e(\text{eff})} = 1.2 \text{ eV}$. Although this is smaller than the peak value of 2.5 eV determined by analyzing the mixer measurements near 380 ns, we note that the OES-derived experimental value was an average $T_{e(\text{eff})}$ acquired for a 10 μs time interval, while the pulsed microwave power was only on for 800 ns. Furthermore, the mixer experimental-1D model results were based on a Maxwellian electron distribution assumption that allowed more high energy electrons in its distribution than the partial Druyvesteyn distribution determined from the OES measurements. Therefore, it is reasonable for the OES measured value to be lower than the

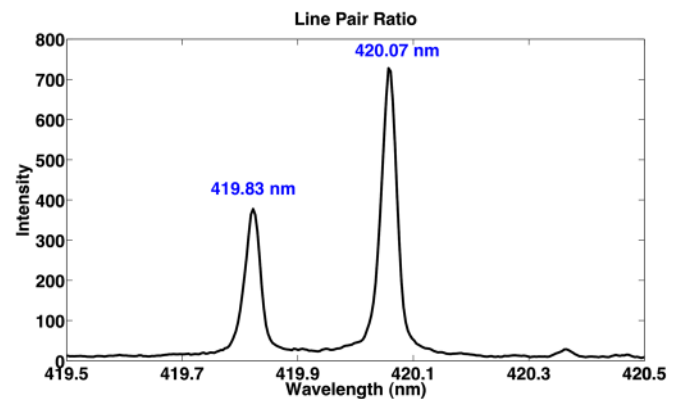


FIG. 8. 420.07 nm/419.83 nm line ratio spectrum when Neon/Argon = 98:2, at 100 Torr. The spectrometer grating is 3600 lines per inch, the gain is 200, and the exposure time is 10 μs with an accumulation number of 800.

value determined by the reflected power and mixer measurements made during the microwave pulse.

V. CONCLUSION

We have shown that for our 15.2 cm long by 14.6 cm diameter cylindrical chamber with polycarbonate end plates mounted flush to the incident X-band waveguide, 43 Hz repetitive pulses (800 ns) at 25.7 kW were sufficient to produce regular, repeatable breakdown in neon in the range of 50 to 250 Torr.

Measurements of the reflected power caused by the plasma showed that the breakdown time at a pressure of 100 Torr for pure neon was 250 ns and once the plasma formed, the reflected power increased dramatically to 70% of the total reflected power measured by inserting a fully reflecting copper disk over the incident polycarbonate window. In addition, by adding a small amount of argon (2%) to the system that allowed Penning discharge breakdown processes to occur, the breakdown time was shortened to 200 ns.

ICCD images using a 50 ns gate time showed that the plasma breakdown and expansion character expanded well beyond the X-band waveguide dimensions. They also allowed us to estimate the maximum plasma thickness as 1 cm. In addition, the ICCD images showed that the plasma optical emission lasted for over 7 μ s, well after the microwave pulse was extinguished. Microwave power transmission measurements received by a single centrally located dipole probe at 31.1 cm from the first polycarbonate window showed a -15 dB received power reduction (97% reflection of the incident power) when the plasma was formed.

By comparing the amplitude and phase of the reflection coefficient measured by microwave diodes and mixers to the six-region, 1-D model, the effective plasma density and electron temperature could be estimated corresponding to an estimated 1 cm maximum plasma thickness. At 100 Torr, under a Maxwellian electron energy distribution assumption, the estimated effective plasma density peaked at 2×10^{12} cm $^{-3}$, while the maximum effective electron temperature was 2.5 eV. Correspondingly, the peak effective collision frequency was 1.1 times the microwave frequency and the peak effective plasma frequency was 1.4 times the microwave frequency. For these high pressure noble gases, these values are consistent with high power microwave ionization and wave penetration processes in collisional, high density, and low electron temperature plasmas.^{14,15}

An OES study of the plasma was conducted to measure the effective electron temperature in Ne/Ar mixture gas by measuring the 420.1 nm/419.8 nm ($3p_9-1s_5/3p_5-1s_4$) neutral line ratios, allowing the determination of different electron distribution functions between a Maxwellian and a Druyvesteyn. At 100 Torr with 2% argon in neon, the line ratio result indicated that the electron energy distribution was not a Maxwellian, but tended somewhat towards a Druyvesteyn distribution that is expected for these highly collisional, unconfined microwave produced plasmas.¹⁹ By assuming an $x = 1.3$ factor in the generalized distribution function, the 10 μ s interval, time averaged effective electron temperature was

determined to be 1.2 eV, smaller than the peak value at 380 ns of 2.5 eV inferred from the mixer experimental measurement.

ACKNOWLEDGEMENTS

This research was supported through AFOSR by a 2009 USDOD multi-university grant on Basic Physics of Distributed Plasma Discharges, Grant No. FA9550-09-1-0086. We thank Dr. Boffard and Professor Wendt for their excellent assistance in helping to set up and interpret our OES measurements.

APPENDIX: WAVE PROPAGATION, ABSORPTION AND REFLECTION MODEL

X-band waveguide TE₁₀ wave impedance

$$\eta_1 = 527 \ \Omega, \quad (\text{A1})$$

$$\beta_1 = 140 \text{ rad/m}. \quad (\text{A2})$$

Air TEM wave impedance

$$\eta_4 = \eta_6 = 377 \ \Omega, \quad (\text{A3})$$

$$\beta_4 = \beta_6 = \omega\sqrt{\epsilon_0\mu_0}. \quad (\text{A4})$$

Polycarbonate material TEM wave impedance

$$\epsilon_r = 2.96, \quad (\text{A5})$$

$$\eta_2 = \eta_5 = \frac{\eta_1}{\sqrt{\epsilon_r}}, \quad (\text{A6})$$

$$\beta_2 = \beta_5 = \beta_1\sqrt{\epsilon_r}, \quad (\text{A7})$$

$$d_2 = d_5 = 0.009525 \text{ m}. \quad (\text{A8})$$

Plasma wave impedance⁵

$$\epsilon_p = \epsilon_0 \left[1 - \frac{\omega_p^2}{\omega(\omega - i\vartheta_{en})} \right], \quad (\text{A9})$$

$$\eta_3 = \sqrt{\frac{\mu_0}{\epsilon_p}}, \quad (\text{A10})$$

$$\beta_3 = j\beta_1 \sqrt{1 - \frac{\omega_p^2}{\omega(\omega - i\vartheta_{en})}}, \quad (\text{A11})$$

$$d_3 = 0.01 \text{ m}. \quad (\text{A12})$$

Frequency: $f = 9.382$ GHz

$$\omega = 2\pi f. \quad (\text{A13})$$

Other parameters

$$\vartheta_{en} = n_0\sigma_{en}v, \quad (\text{A14})$$

$$v = \sqrt{\frac{kT_e}{m}}, \quad (\text{A15})$$

$$n_0 = 3.25 \times 10^{-16} * P \text{ (P is the gas pressure)}. \quad (\text{A16})$$

Cross section for neon¹³ σ_{en}

$$\sigma_{en} = \begin{cases} 1.23 \times 10^{-16} \text{ cm}^2 & (T_e = 10 \text{ eV}) \\ 1.06 \times 10^{-16} \text{ cm}^2 & (T_e = 1 \text{ eV}). \end{cases} \quad (\text{A17})$$

For T_e values between 2 eV and 5 eV, the relationship between σ_{en} and T_e can be expressed as a linear function¹³

$$\sigma_{en} = (0.2657T_e + 1.5171) \times 10^{-20} \text{ m} \quad (T_e \text{ is in eV}). \quad (\text{A18})$$

1. Reflection coefficients

$$\eta_{56} = \eta_2 \frac{\eta_1 + j\eta_2 \tan(\beta_2 d_2)}{\eta_2 + j\eta_1 \tan(\beta_2 d_2)}, \quad (\text{A19a})$$

$$\eta_{456} = \eta_1 \frac{\eta_{56} + j\eta_1 \tan(\beta_1 d_4)}{\eta_1 + j\eta_{56} \tan(\beta_1 d_4)}, \quad (\text{A19b})$$

$$\eta_{3456} = \eta_3 \frac{\eta_{456} + \eta_3 \tanh(\beta_3 d_3)}{\eta_3 + \eta_{456} \tanh(\beta_3 d_3)}, \quad (\text{A19c})$$

$$\eta_{23456} = \eta_2 \frac{\eta_{3456} + j\eta_2 \tan(\beta_2 d_2)}{\eta_2 + j\eta_{3456} \tan(\beta_2 d_2)}, \quad (\text{A19d})$$

$$\Gamma = \frac{\eta_{23456} - \eta_1}{\eta_{23456} + \eta_1}. \quad (\text{A19e})$$

Reflection power attenuation = $20 \log|\Gamma|$.²⁰

2. Transmission coefficients

$$\Gamma_{56} = \frac{\eta_1 - \eta_2}{\eta_1 + \eta_2}, \quad (\text{A20a})$$

$$\Gamma_{46} = \frac{\eta_{56} - \eta_1}{\eta_1 + \eta_{56}}, \quad (\text{A20b})$$

$$\Gamma_{36} = \frac{\eta_{456} - \eta_3}{\eta_{456} + \eta_3}, \quad (\text{A20c})$$

$$\Gamma_{26} = \frac{\eta_{3456} - \eta_2}{\eta_{3456} + \eta_2}, \quad (\text{A20d})$$

$$t_{56} = \frac{2\eta_1}{\eta_2 + \eta_1}, \quad (\text{A20e})$$

$$t_{46} = \frac{1 + \Gamma_{46}}{e^{i\beta_2 d_2} + \Gamma_{56} e^{-i\beta_2 d_2}}, \quad (\text{A20f})$$

$$t_{36} = \frac{1 + \Gamma_{36}}{e^{i\beta_1 d_4} + \Gamma_{46} e^{-i\beta_1 d_4}}, \quad (\text{A20g})$$

$$t_{26} = \frac{1 + \Gamma_{26}}{e^{\beta_3 d_3} + \Gamma_{36} e^{-\beta_3 d_3}}, \quad (\text{A20h})$$

$$t_{16} = \frac{1 + \Gamma}{e^{i\beta_2 d_2} + \Gamma_{26} e^{-i\beta_2 d_2}}, \quad (\text{A20i})$$

$$T = t_{56} t_{46} t_{36} t_{26} t_{16}. \quad (\text{A20j})$$

Transmission power attenuation = $20 \log|T|$.²⁰

¹A. D. MacDonald, *Microwave Breakdown in Gases* (John Wiley and Sons, Inc., New York, 1966).

²D. Holmquist, M. Kirley, C. Cook, J. Scharer, and J. Booske, in *IEEE International Vacuum Electronics 2010: Proceedings of 11th International Vacuum Electronics Conference, Monterey, CA, USA, 18 May–20 May 2010*.

³K. M. Green, M. C. Borrás, P. P. Woskov, G. J. Flores III, K. Hadidi, and P. Thomas, *IEEE Trans. Plasma Sci.* **29**, 399 (2001).

⁴S. R. Beeson, P. J. Ford, J. Foster, H. G. Krompholz, and A. A. Neuber, *IEEE Trans. Plasma Sci.* **39**, 2600 (2011).

⁵M. A. Lieberman and A. J. Lichtenberg, *Principles of Plasma Discharges and Materials Processing* (John Wiley and Sons, Inc., New Jersey, 2005), p. 96.

⁶B. Kupczyk, C. H. Liu, X. Xiang, J. Scharer, N. Behdad, and J. Booske, in *IEEE Pulsed Power & Plasma Science 2013: Proceedings of the 40th International Conference on Plasma Science, San Francisco, USA, 16 June–21 June 2013*, edited by B. Oliver (Sandia National Laboratories, 2013), p. 121.

⁷J. S. Hummelt, M. A. Shapiro, and R. J. Temkin, *Phys. Plasmas* **19**, 123509 (2012).

⁸C. O. Laux, R. J. Gessman, C. H. Kruger, F. Roux, F. Michaud, and S. P. Davis, *J. Quantum Spectrosc. Radiat. Transfer* **68**, 473–482 (2001).

⁹K. H. Becker, U. Kogelschatz, K. H. Schoenbach, and R. J. Barker, *Non-equilibrium Air Plasmas at Atmospheric Pressure* (Taylor & Francis, London, 2005).

¹⁰C. O. Laux, Ph.D. thesis, Stanford University, 1993.

¹¹C. O. Laux, T. G. Spencer, C. H. Kruger, and R. N. Zare, *Plasma Sources Sci. Technol.* **12**, 125 (2003).

¹²S. Luo, C. M. Denning, and J. E. Scharer, *J. Appl. Phys.* **104**, 013301 (2008).

¹³A. Zecca, G. P. Karwasz, and R. S. Brusa, *La Rivista Nuovo Cimento* **19**(3), 1 (1996).

¹⁴J. Torres, J. M. Palomares, A. Sola, J. J. A. M. van der Mullen, and A. Gamero, *J. Phys. D: Appl. Phys.* **40**, 5929–5936 (2007).

¹⁵S. Beeson, J. Dickens, and A. Neuber, *Phys. Plasmas* **20**, 093509 (2013).

¹⁶J. B. Boffard, R. O. Jung, C. C. Lin, L. E. Aneskavich, and A. E. Wendt, *J. Phys. D: Appl. Phys.* **45**, 045201 (2012).

¹⁷V. M. Donnelly, *J. Phys. D: Appl. Phys.* **37**, R217–R236 (2004).

¹⁸J. B. Boffard, R. O. Jung, C. C. Lin, and A. E. Wendt, *Plasma Sources Sci. Technol.* **19**, 065001 (2010).

¹⁹S. K. Nam and J. P. Verboncoeur, *Appl. Phys. Lett.* **93**, 151504 (2008).

²⁰C. A. Balanis, *Advanced Engineering Electromagnetics* (John Wiley and Sons, Inc., New York, 1989).

